# AERODYNAMIC FORCES OF A COANDA AIR JET

by

**E. Y. Hong and Y. B. Chang**
**Oklahoma State University**
**USA**

## ABSTRACT

This paper discusses the aerodynamic pressure and frictional force on a plate (called web) placed against a plane wall jet of air. The air jet was ejected from a slot nozzle, turned 90 degrees following a curved surface, and then flew along a straight wall. The tendency of a jet flow to follow a contoured surface is commonly called the Coanda effect. The aerodynamic forces were determined for rigid and flexible webs, experimentally and computationally. A commercial computational fluid dynamics package, called Fluent, was used. For a flexible web, solutions which satisfied both the fluid dynamics and web deflection equations were obtained by manual iteration. Effects of the supply air pressure in the plenum of the air nozzle, floatation height (distance between the web and the nozzle surface), slot nozzle width (opening), radius of curvature of the curved surface, and applied web tension (for flexible web) on the aerodynamic forces on the web were examined. It was found that the aerodynamic pressure is very sensitive to the flotation height. For a stationary rigid web, the net lift force became nearly zero at a certain value of flotation height regardless of supply pressure. The magnitude of pressure on the web and friction were nearly proportional to the supply pressure in the entire range of measurements and computations. The effect of web speed on the aerodynamic friction was examined computationally. It was found that the frictional force dramatically reduces when the web runs in the direction of air jet. An analytical model to predict the aerodynamic traction on the web was developed. The analytical model, however, was only limited to a stationary rigid web.

## INTRODUCTION

Thin, flexible materials such as paper, plastic films, metal foils, and fabrics are widely called webs. When manufacturing extremely soft web materials at high speeds (for example, tissue products running at 30 m/s (6000 fpm) or faster), the aerodynamic drag may not be negligibly small compared to the web tension. In such situations, high-

speed air jets can be used to generate the aerodynamic traction in the direction of web motion (machine direction) and thus maintain the tension constant along the machine direction. Air jets can also be used to propel web materials for the purpose of full-speed threading of paper machines or handling webs at extremely low tension.

One method of generating aerodynamic traction on the web material is to use the Coanda effect, which is described as a tendency of fluid to follow a contoured surface. There are many interesting applications of the Coanda effect. Those readers who are interested in the Coanda effect and its applications may refer to Squire (1950), Newman (1961), Wille and Fernholz (1965), Reba (1966), and Wilson and Goldstein (1976).

The purpose of this paper is to describe our efforts for determination of the aerodynamic forces on the web generated by a Coanda air jet. An attempt for the development of an analytical model is explained first. A commercial code, called Fluent, was used for computations, and the results were compared with experiments

## THEORETICAL ANALYSES

Consider the air flow ejected from the slot of a Coanda air nozzle and flowing through the gap under the web. The cross section of the system is shown in Figure 1, where the air jet flows to the right.

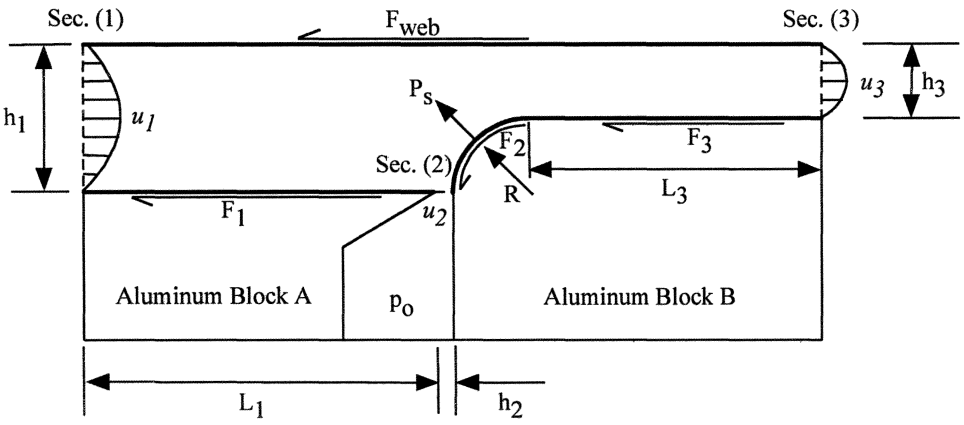


**Figure 1. Control volume**

The conservation of mass for the system is stated as

$$Q = h_1\overline{u_1} + h_2\overline{u_2} = h_3\overline{u_3} \qquad \{1\}$$

where the upper bar indicates an average value. By the Newton's second law, resultant force on the control volume must be the same as the change in the momentum flux:

$$\frac{\partial}{\partial t}\int_{CV} u_x \rho dV + \int_{CS} u_x \rho \vec{v}\cdot\hat{n}dA = \sum F_x \qquad \{2\}$$

where x indicates the horizontal direction of the control volume. The first term can be ignored because the flow is assumed to be steady. The second term, which is the change in x-component of momentum flux, can be expressed as

$$\int_{CS} u\rho\vec{v}\cdot\hat{n}dy = -\rho\int_{sec1} u^2 dy + \rho\int_{sec3} u^2 dy \qquad \{3\}$$

where $dA$ was changed to $dy$ to consider the flow and force per unit depth. The right hand side term of equation {2}, which is the resultant force on the control volume per unit depth can be written as

$$\sum F_x = -F_p - F_1 - F_2 - F_3 - F_{web} \qquad \{4\}$$

where $F_p$ is horizontal component of pressure force acting on the curved portion of the nozzle surface downstream the knife edge, $F_1$ and $F_3$ present the drag on the horizontal portion of the nozzle surface after the curved portion of the nozzle, and $F_2$ presents the horizontal component of the drag on the curved surface. If we substitute equations {3} and {4} into equation{2}, the traction on the web can be expressed as

$$F_{web} = -F_p - F_1 - F_2 - F_3 + \rho\int_{sec1} u^2 dA - \rho\int_{sec3} u^2 dA \qquad \{5\}$$

The flow velocity profile at Section 1 and Section 3 are assumed to be fully developed. The surface pressure distribution developed by Newman (1961) was used to evaluate $F_p$. $F_1$ and $F_3$ were found with the assumption that the flow is fully developed. The skin friction coefficient for the curved jets proposed by Kobayashi and Fujisawa (1983) was used to obtain $F_2$. The values of air density and viscosity are at standard atmospheric pressure and 20 °C ( $\rho = 1.20$ kg/m$^3$ and $\mu = 1.80\times10^{-5}$ N·s/m$^2$ ).

One of the most difficult part of the analysis is to determine the flotation height of the web, which is the equilibrium position of the web. One way to define the flotation height is

$$h_3 = \left.\frac{Q}{\bar{u}}\right|_{sec3} \qquad \{6\}$$

In this study, the average velocity is assumed $\bar{u} = 2u_{max}/3$, which is for a fully developed, laminar, channel flow. The maximum flow velocity, $u_{max}$, is in turn unknown. Based on the measured traction data for the flexible web, it was assumed that the maximum velocity at Section 3 is 1.6 times the maximum velocity at the position where the curvature of the nozzle ends, which can be found from the equation developed for a free curved wall jet (without the presence of web) by Wilson and Goldstein (1976). The flow rate of jet stream was found by integrating the self-similar velocity profiles of inner and outer layer on the curved wall, which were proposed by Rodman, Wood, and Roberts (1989). The flow rate at the slot nozzle was calculated assuming that the discharge coefficient is 0.6. The entrained air through Section 1 is, based on the principle of mass conservation, the same as the exiting air flow rate at Section 3 minus the incoming flow rate through Section 2. When we consider typical test conditions to be explained later (b = 0.254 mm = 0.01 in, R = 4.37 mm = 11/64 in), the flotation height becomes H = 1.58 mm (0.0623 in).

Predicted traction on the web for various values of nozzle opening is shown in Figure 2, and the effects of the radius of curvature on traction are shown in Figure 3. The effects of the radius of curvature on flotation height are shown in Figure 4, and the effects of nozzle openings on flotation height are shown in Figure 5. When the nozzle opening

is large or when the radius of curvature is large, higher traction on the web is predicted. It is seen that the traction dramatically increases with the nozzle opening. The flotation height of the web over the air jet is determined by the curvature of the nozzle and nozzle opening not by the supply pressure.

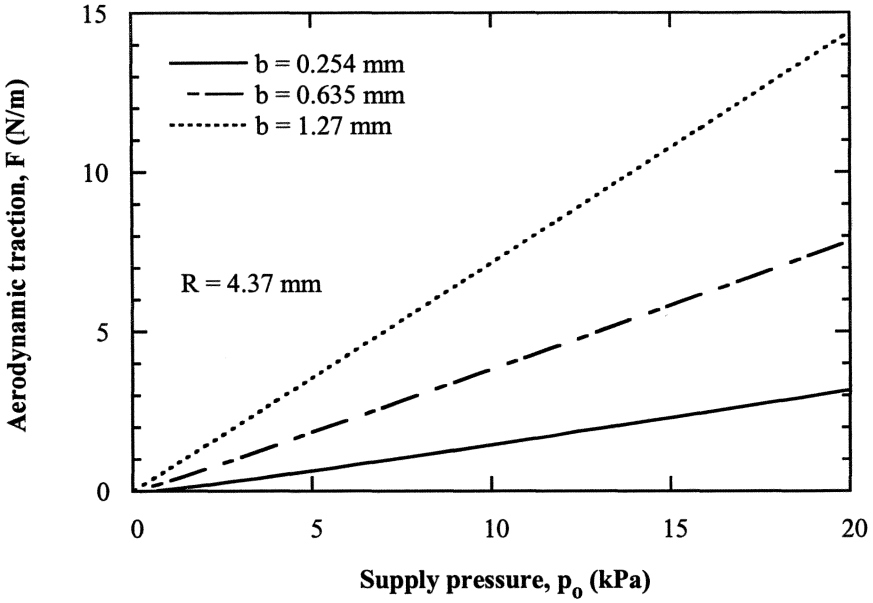


**Figure 2. Effects of slot nozzle on predicted traction**

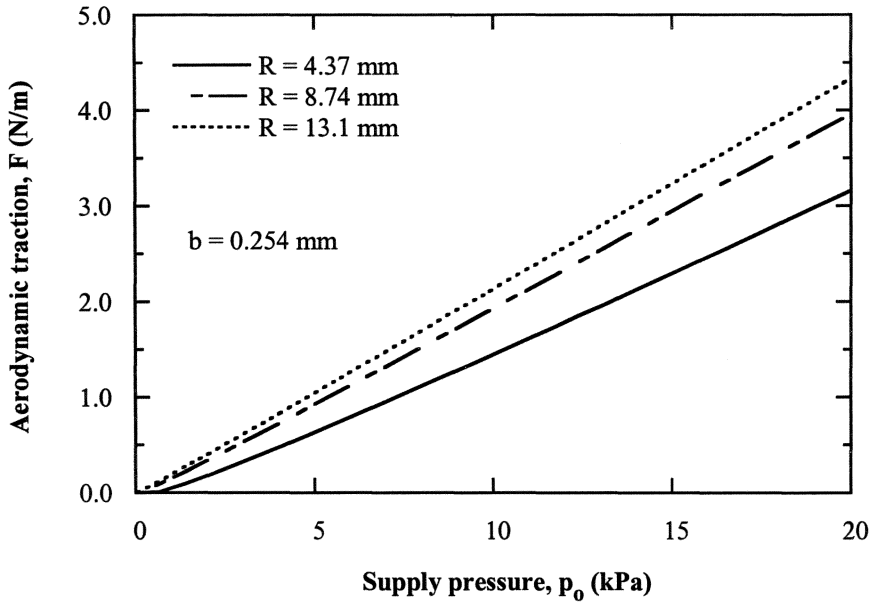


**Figure 3. Effects of radius of curvature predicted traction**

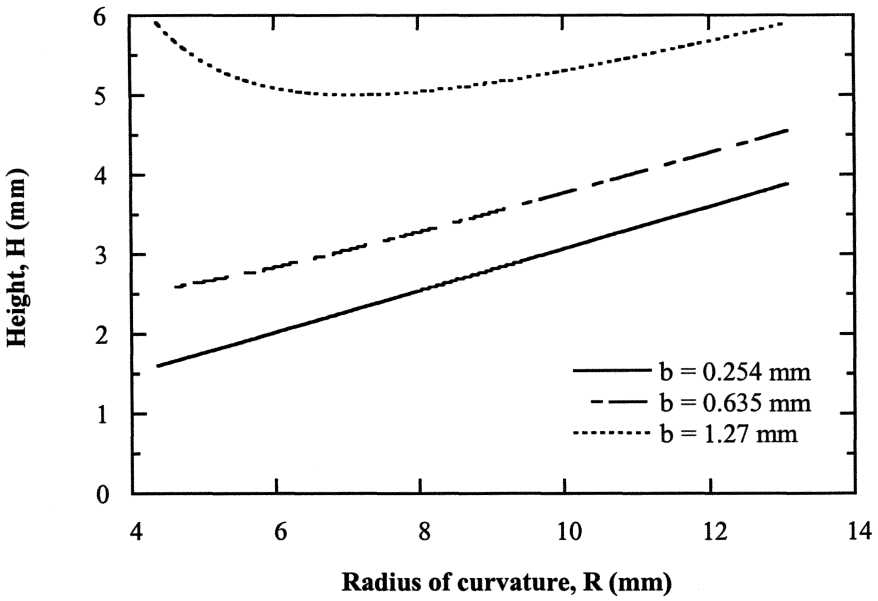


**Figure 4. Effects of radius of curvature on flotation height**

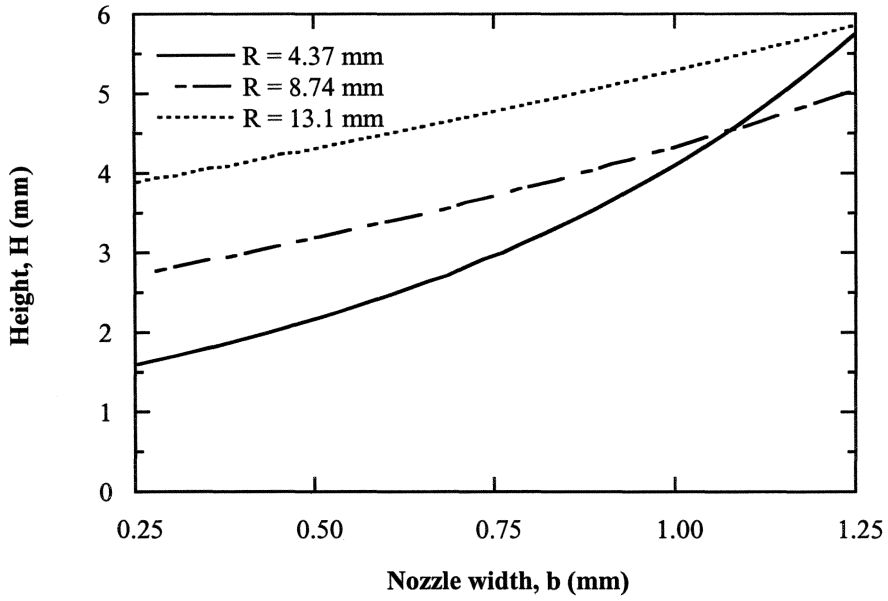


**Figure 5. Effects of nozzle openings on flotation height**

## COMPUTATIONS

FLUENT (V5.5) was used for computations of aerodynamic forces on the web. In this study, the flow was assumed to be a two dimensional, compressible, and steady flow. The unstructured quadrilateral grid was used. For turbulence viscous model, either the Realizable $k-\varepsilon$ model or Reynolds Stress Model was selected depending on the difficulty of convergence with the Two-Layer Zonal Model for the near wall treatment. In the Two-Layer Zonal Model, the turbulence models were modified to enable the viscosity-affected region to be resolved with a mesh all the way to the wall, including the viscous sublayer. Second order upwind scheme was used for interpolation between grid points and to calculate derivatives of the flow variables.

### Coanda Air Jet and a Stationary Rigid Web

The computational model shown in Figure 6 simulates the experimental model shown in Figure 20. Pressure outlet boundaries are the surfaces where the total pressure in constant, which is the atmospheric pressure in this study. The right-hand side pressure boundary was placed 2.03 meters (80 in) downstream of the slot nozzle, and the left-hand side pressure boundary was placed 1.02 meters (40 in) upstream of the slot nozzle. The mesh had 216,487 cells over the computational domain (Figure 7), and 3450 cells at the wall that simulated the web (Section AD in Figure 6). Normally the number of iterations to convergence was 1500 - 2500 for a residual value of $1\times10^{-5}$, which was used as the criterion for convergence.

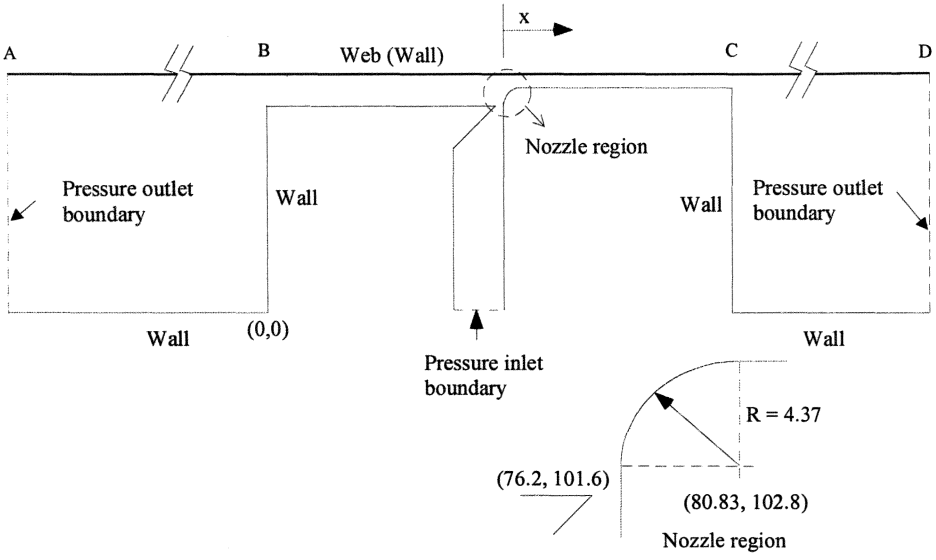


**Figure 6. Computational model (in mm)**

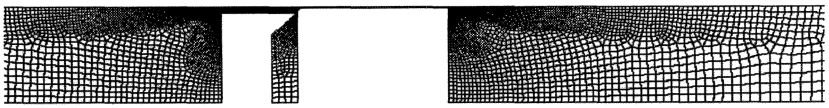


**Figure 7. Overall Mesh**

Pressure profiles on the rigid web are shown for various flotation heights for $p_o$ = 6.89 kPa (1 psig) (Figure 8). This figure clearly shows that the location where the static pressure becomes maximum shifts downstream as the flotation height increases.

The lift force (per unit width of web) is obtained by integrating the pressure profile. Figure 9 and Figure 10 show the dependence of lift force on supply air pressure and flotation height. When the flotation height is small (H = 2.54 mm = 0.10 in), the lift force is positive in the entire range of test and increases with the supply pressure. At a large value of flotation height (H = 10.2 mm = 0.40 in), the lift force is negative, and its magnitude increases with the supply pressure. It appears that there is a value of flotation height, near H = 6.35 mm (0.25 in), at which the lift force becomes zero without being affected by the supply pressure. That flotation height is the equilibrium position of a rigid, non-tilted, web with a nozzle width of b = 0.254 mm (0.01 in).

By integrating the shear stress profiles along the flow direction, the aerodynamic traction (force per unit width) was obtained for various values of flotation height and supply air pressure as shown in Figure 11. The trapezoidal method was used to perform this integration. It is seen that the aerodynamic traction on the web is almost proportional to the supply air pressure. It is also seen that the effect of the supply pressure is more dramatic when the flotation height is small. Refer to Table 1 for exact values of the data.

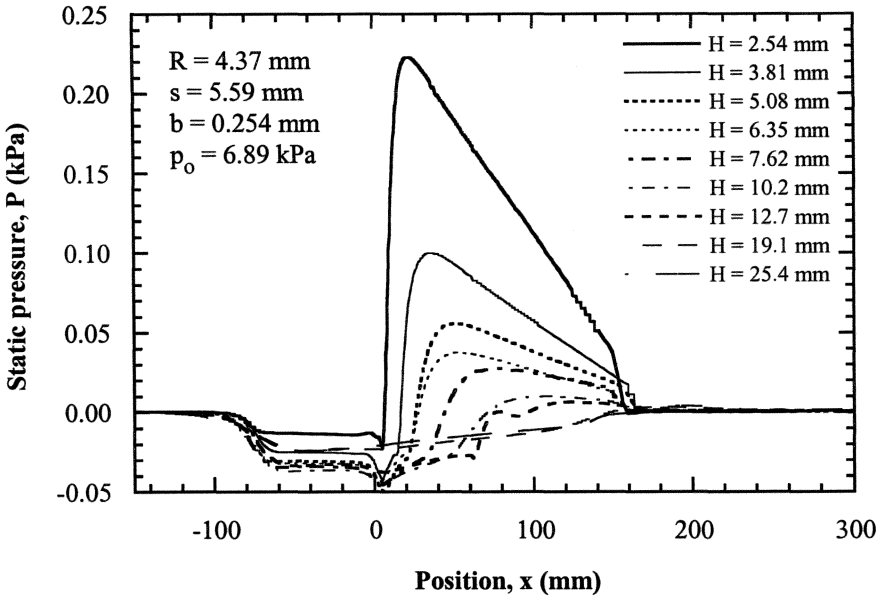


**Figure 8. Pressure distribution on the web for different flotation heights**

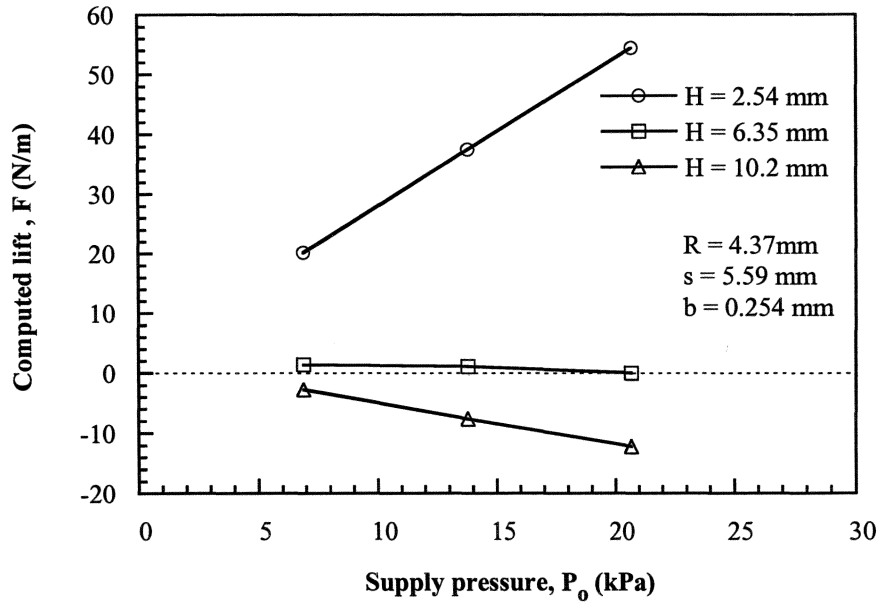


**Figure 9. Effects of supply pressure and flotation height on lift force**

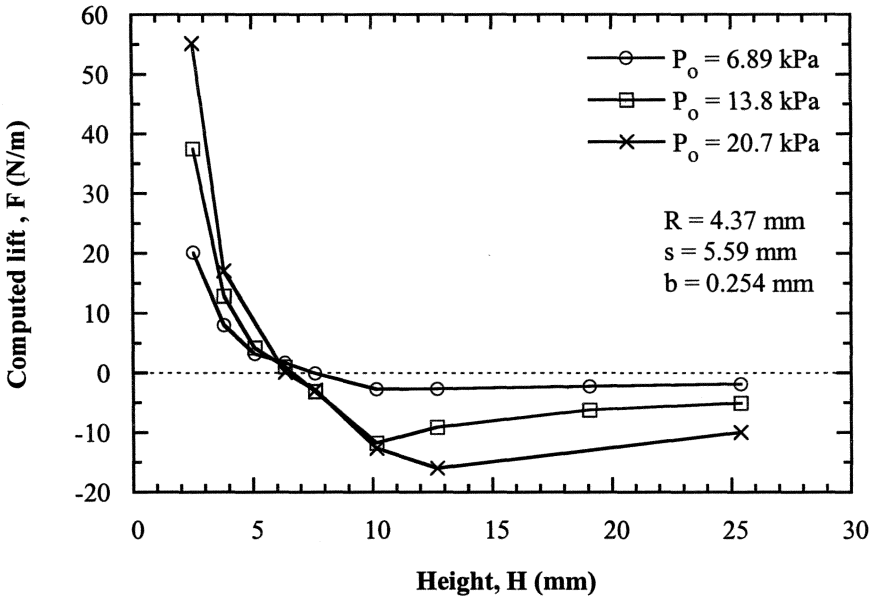


**Figure 10. Effects of flotation height and supply pressure on lift force**

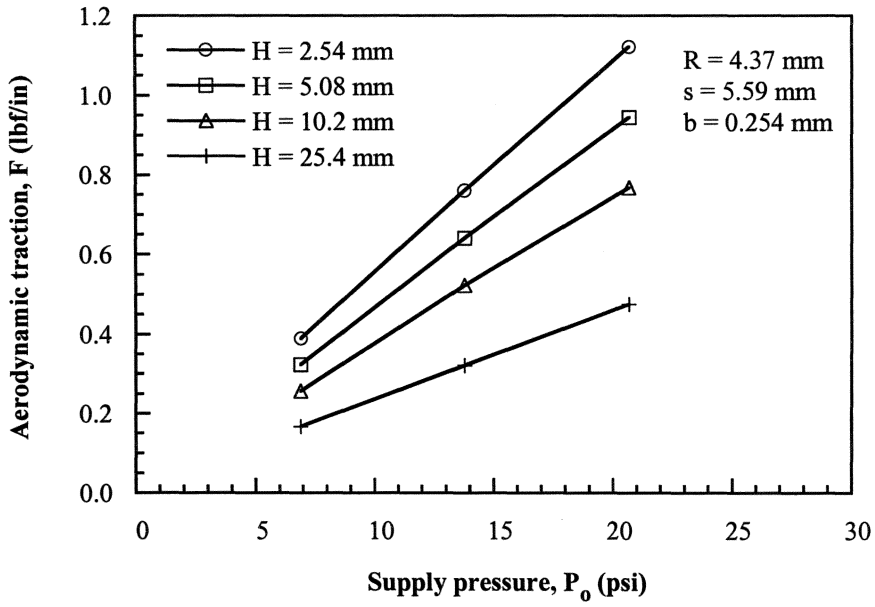


**Figure 11. Effects of supply pressure and flotation height on traction**

**Table 1. Computed aerodynamic traction on a stationary rigid web for various supply pressures and flotation heights (N/m)**

| | H = 1.58 mm | H = 2.54 mm | H = 5.08 mm | H = 10.16 mm | H = 25.40 mm |
|---|---|---|---|---|---|
| $p_o$ = 6.89 kPa | 0.5814 | 0.3888 | 0.3222 | 0.2557 | 0.1671 |
| $p_o$ = 13.8 kPa | 1.1471 | 0.7601 | 0.6410 | 0.5219 | 0.3205 |
| $p_o$ = 20.7 kPa | 1.9790 | 1.1208 | 0.9440 | 0.7671 | 0.4746 |

**Coanda Air Jet and a Moving Rigid Web**

The model is almost the same as the previous one, except that the web translates in horizontal direction. As shown in Figure 12, the lift force on the web decreases as the web speed increases. This implies that the equilibrium position of a translating rigid web will be lower than that of a stationary web. This effect becomes less prominent at high supply pressure (20.7 kPa), which can be expected because the speed ratio ($U_{web} / V_{jet}$) decreases with the supply pressure.

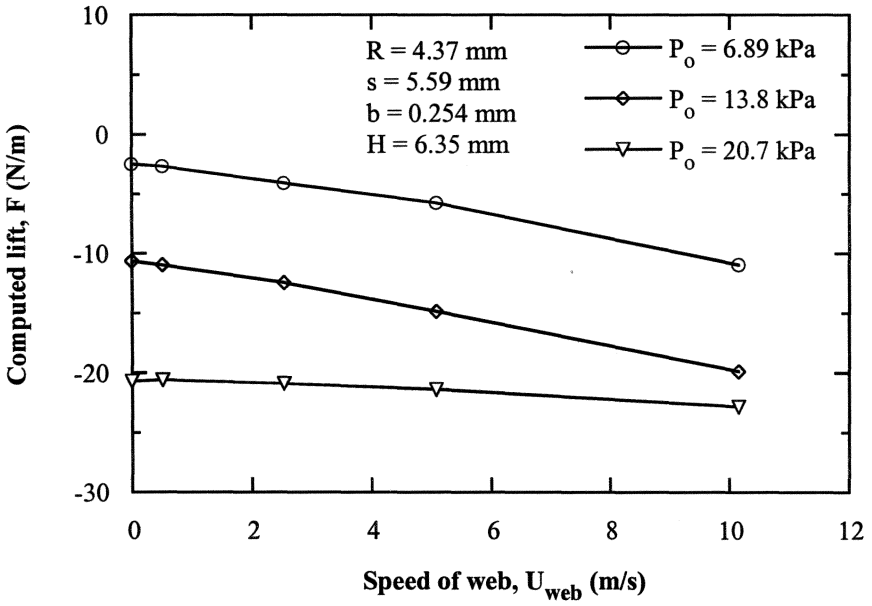


**Figure 12. Effects of speed of web and supply pressure on lift force**

Integrating the wall shear stress over the web gives the traction on the web (frictional force per unit width). As seen in Figure 13, the traction of the air jet decreases as the speed of web increases. The effect of web speed on the aerodynamic traction becomes less significant when the supply air pressure is high. The results are tabulated in Table 2.

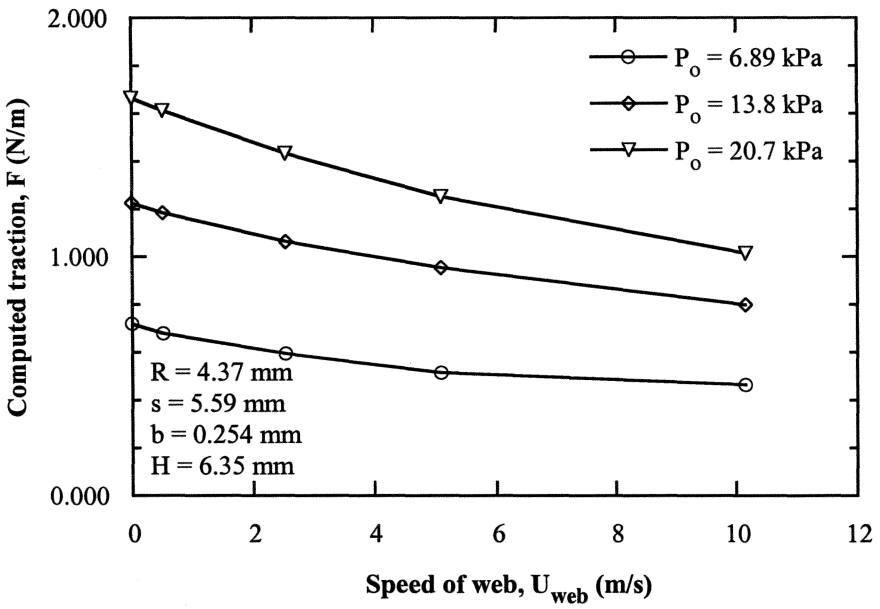


**Figure 13. Traction on the moving rigid web**

**Table 2. Computed aerodynamic traction on the moving rigid web for various supply pressures and speeds of web (N/m)**

| | $U_{web}$ = 0 m/s | $U_{web}$ = 0.508 m/s | $U_{web}$ = 2.54 m/s | $U_{web}$ = 5.08 m/s | $U_{web}$ = 10.2 m/s |
|---|---|---|---|---|---|
| $p_o$ = 6.89 kPa | 0.7180 | 0.6795 | 0.5937 | 0.5149 | 0.4553 |
| $p_o$ = 13.8 kPa | 1.2259 | 1.1839 | 1.0630 | 0.9545 | 0.8056 |
| $p_o$ = 20.7 kPa | 1.6637 | 1.6129 | 1.4326 | 1.2504 | 1.0158 |

**Coanda Air Jet and a Stationary Flexible Web**

A flexible web was placed above the Coanda nozzle, and the model simulates a situation in which the Coanda air jet is used for generating the aerodynamic traction in the machine direction. A flexible web can be modeled as a plate, and its equilibrium equation for a flexible web can be expressed as

$$D\frac{d^4w}{ds^4} - T\frac{d^2w}{ds^2} = p_1 - p_2 \qquad \{7\}$$

where $w$ is the web displacement, $D = \frac{Et^3}{12(1-\nu^2)}$ is the bending stiffness, $t$ is the web thickness, $\nu$ is Poisson's ratio, $T$ is the web tension, $p_1$ is the pressure on the side affected by the air jet, and $p_2$ is the ambient pressure.

The web boundary conditions are

$$w\big|_{s=0} = 0, \quad \left.\frac{dw}{ds}\right|_{s=0} = 0, \quad w\big|_{s=L} = 0, \quad \left.\frac{dw}{ds}\right|_{s=L} = 0 \qquad \{8\}$$

Once the pressure distribution and web tension are known, the out-of-plane deflection profile of the web can be obtained. Then the flow and pressure profiles are calculated based on the newly calculated web deflection profile. This interactive procedure is repeated to obtain the solution that satisfies both fluid dynamics and web deflection equations. Web deflection profiles for various values of applied tension are shown in Figure 14. Note that the scales of two axes are much different.

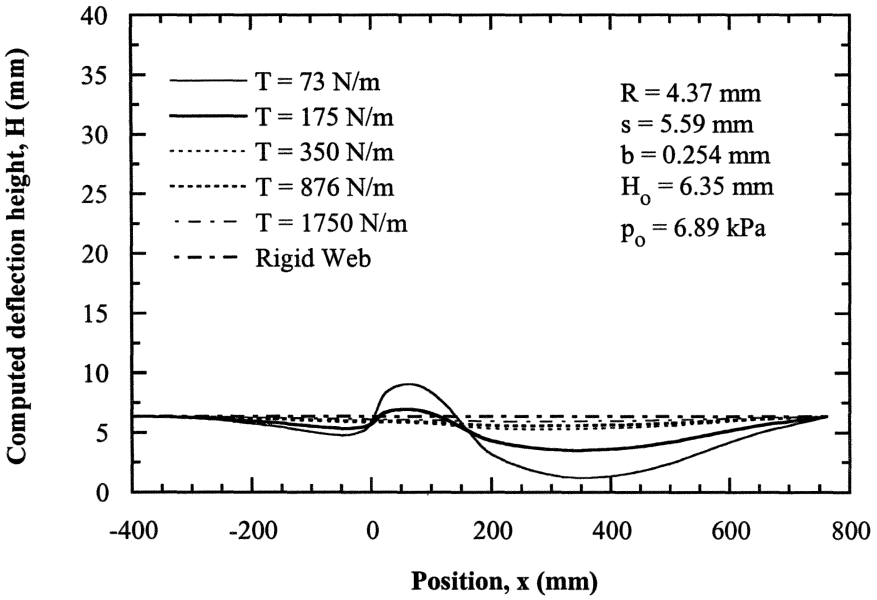


**Figure 14. Deflection profile of the flexible web for different applied tensions**

The aerodynamic traction tends to increase with web tension when the tension is low, but the effect of tension becomes negligible at higher tension (Figure 15). Web tension affects the pressure profile on the web and also the lift force, which is an integrated pressure along the machine direction (Figure 16 and Figure 17). It is seen that the suction force increases with tension.

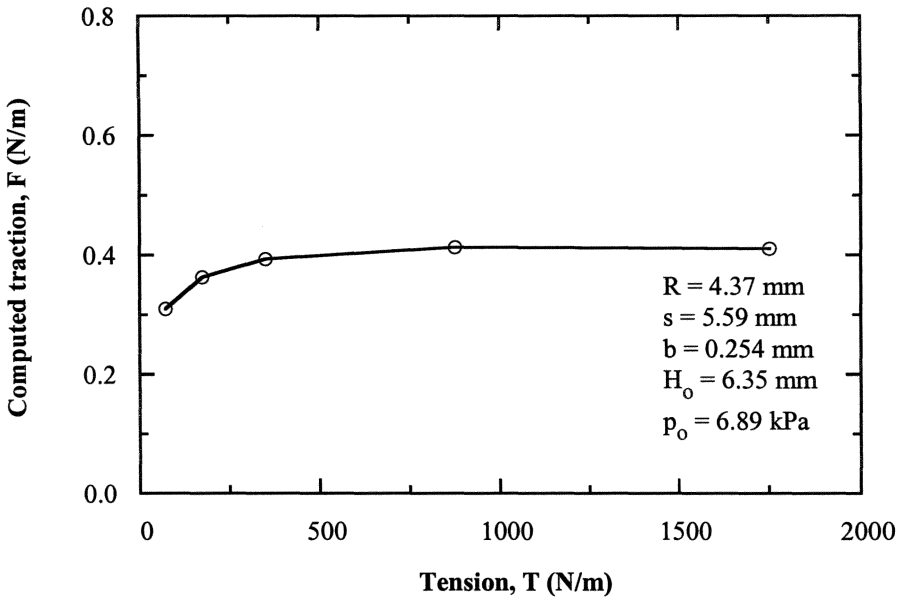


**Figure 15. Effect of applied tension on traction**

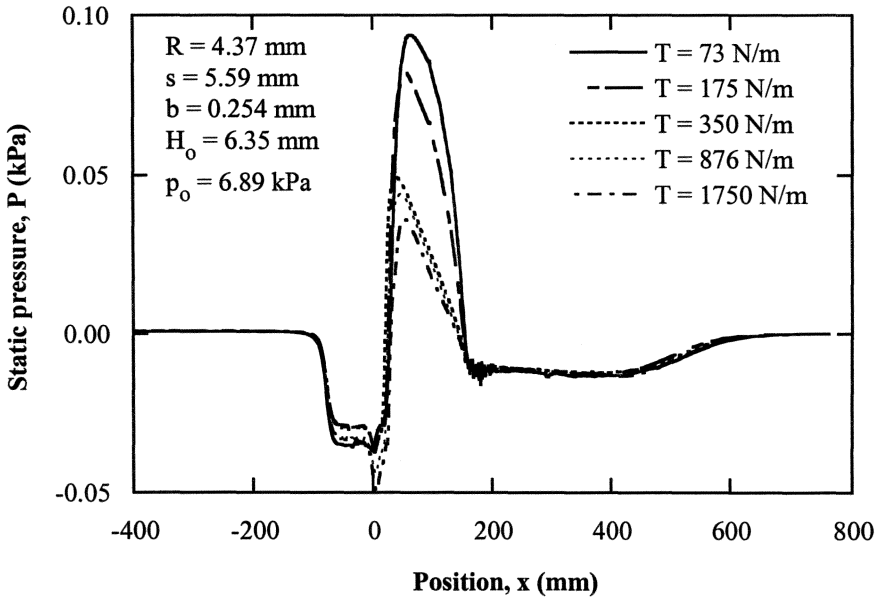


**Figure 16. Effects of web tension on pressure distribution**

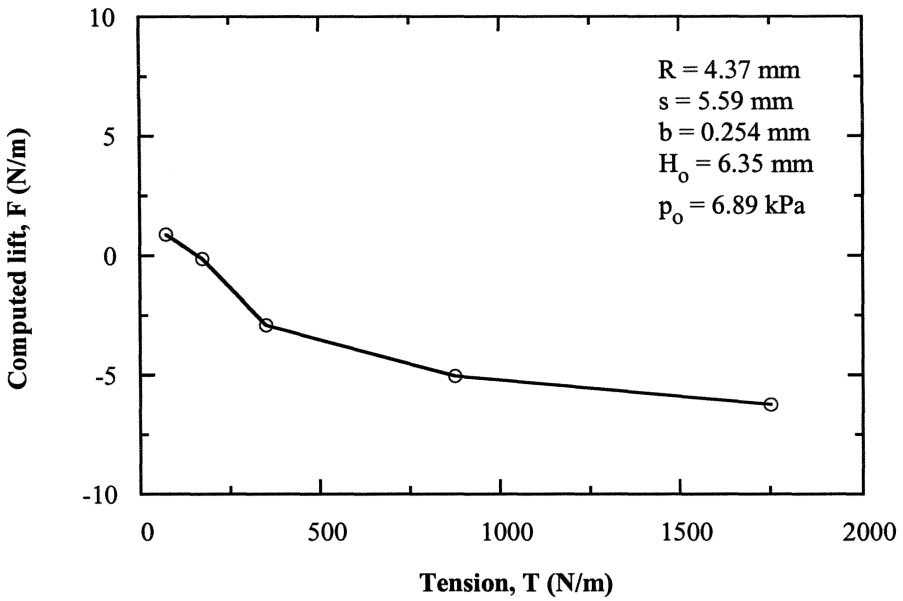


**Figure 17. Effect of applied tension on lift force**

## EXPERIMENTS

The setup consisted of a Coanda nozzle, a traversing table, a steel frame, a flexible web (plastic film), and the instruments including a load cell and a pressure transducer. The schematic of the Coanda nozzle is shown in Figure 18. One main component of the test setup was the aluminum block with a sharp edge (A in Figure 18), which was 0.203 meters (8 in) high, 0.152 meters (6 in) deep, and 0.076 meters (3 in) long (in the horizontal direction). The knife edge of the block had an angle of about 45°, and the nozzle width was adjustable. The other aluminum block (B) had a 90° turning convex surface with the radius of curvature of 4.37 mm (11/64 in). Dimensions of the curved surface block were 0.102 meters (4 in) in height, 0.152 meters (6 in) in depth, and 0.0508 meters (2 in) in length (horizontal dimension). A flap, 0.102 meters (4 in) in length, was attached to block B to increase the effective length of the block.

The two side plates were extended about 0.0889 meters (3.5 in) above the top surface of the nozzle to make air dams for maintaining a two-dimensional flow field. Compressed air was supplied to the settling chamber through two air inlets and ejected through the slot nozzle. The settling chamber was filled with a porous material to make the air flow uniform.

A 0.0762 mm (0.003 in) thick plastic film was used for the web. The web was supported by two air bars, 0.0508 meters (2 in) in diameter, mounted on the steel frame as shown in Figure 19 and Figure 20. The purpose of supporting the web with air bars was to allow the web to move in the longitudinal direction without friction. The pressure on the web affected the out-of-plane defection profile of the web, which in turn caused longitudinal sliding of the web at the supports. Any friction at the supports would cause an error in the measurement of the aerodynamic traction. Because of the friction-free supports (air bars) and flutter of the web, the flexible web sometimes touched the air

dams during the test. A load cell was fixed on the rigid bottom plate, and its top was fixed to the end of the web by a vertical rod and a string as shown in Figure 20. A micrometer was mounted on the steel frame to measure the out-of-plane deflections of the web at selected points. Two identical weights were attached at the two ends of the web to apply web tension. A change of the force on the load cell caused by the air jet was measured.

Before the test was conducted, the load cell was calibrated using dead weights in the range of 0.0 to 0.278 N (0.0625 lbf) in compression mode in the same way as for the rigid-web test. The setup was aligned carefully so that the web would not touch the air dams. Another important parameter for the flexible-web test was the height of web supports (air bars). After all the parameters were adjusted and checked, the zero correction value of the load cell was input into the data acquisition program. The supply air pressure was increased to a predetermined value and all the readings were taken. At the same time, the out-of-plane deflection of the web at some locations was measured using the micrometer at some locations. The main test variables were the supply air pressure, width of the nozzle, and tension. The test conditions are tabulated in Table 3.

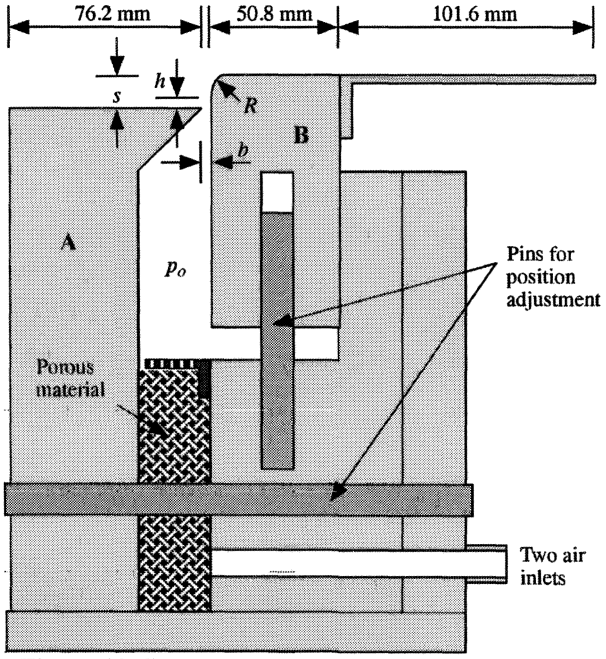


**Figure 18. Schematic of the Coanda air nozzle**

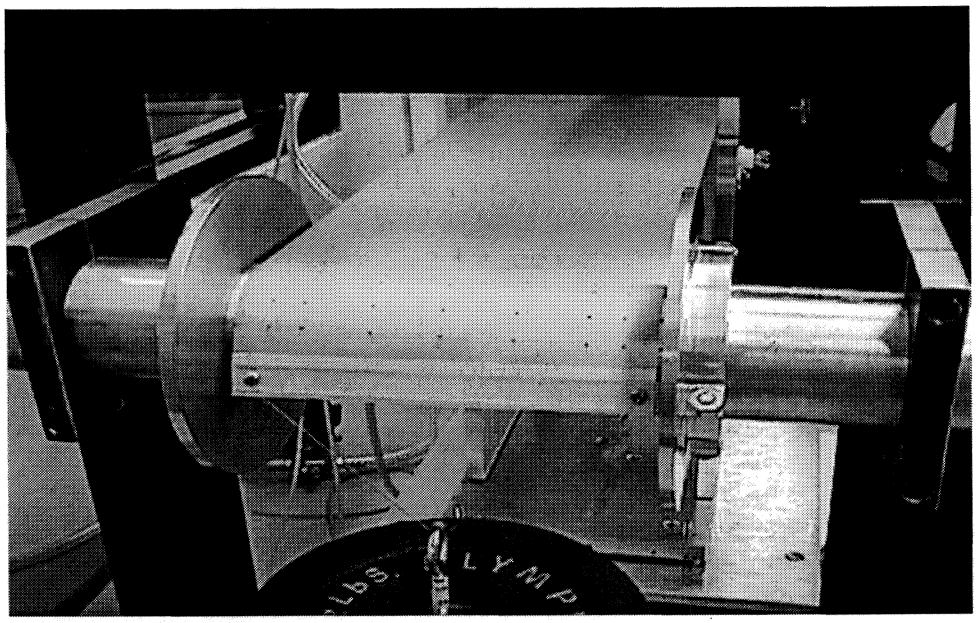

**Figure 19. Non-contact support of the flexible web**

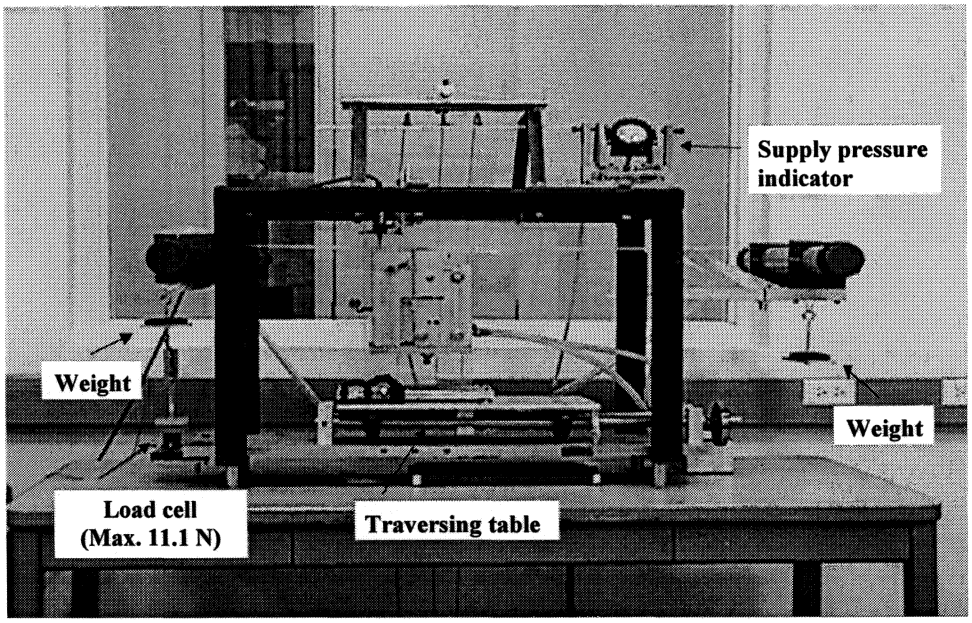


**Figure 20. Side view of the flexible-web test setup**

**Table 3. Flexible-web test conditions**

| Parameter | Symbol | Value |
|---|---|---|
| Radius of curvature | R | 4.37 mm |
| Nozzle offset | s | 5.59 mm |
| Nozzle width | b | 0.254 - 1.27 mm |
| Height of air bar | $H_0$ | 2.92 mm |
| Supply pressure | $p_o$ | 6.89 - 24.1 kPa |

## COMPARISONS

The computed pressure profile on the rigid web is compared with the measured profile for the flotation height of H = 6.35 mm (0.25 in) in Figure 21. The two results show a similar trend, but the computed static pressure profile tend to be higher than the measured results. For the flotation height of H = 5.08 mm (0.20 in), the computed and measured traction results agree reasonably well within the range of calculation (Figure 22 and Figure 23). The non-dimensional traction ($F/p_o b$) on the rigid web for H = 5.08 mm (0.20 in) was approximately 0.2.

Figure 24 and Figure 25 show the measured, computed, and predicted tractions on the web for various values of the supply pressures. The measured and predicted values of traction for the range of the supply pressures (6.89 to 20.7 kPa (1 to 3 psig)) seem to be close to each other. The computational results are lower than the results of experiment and analysis.

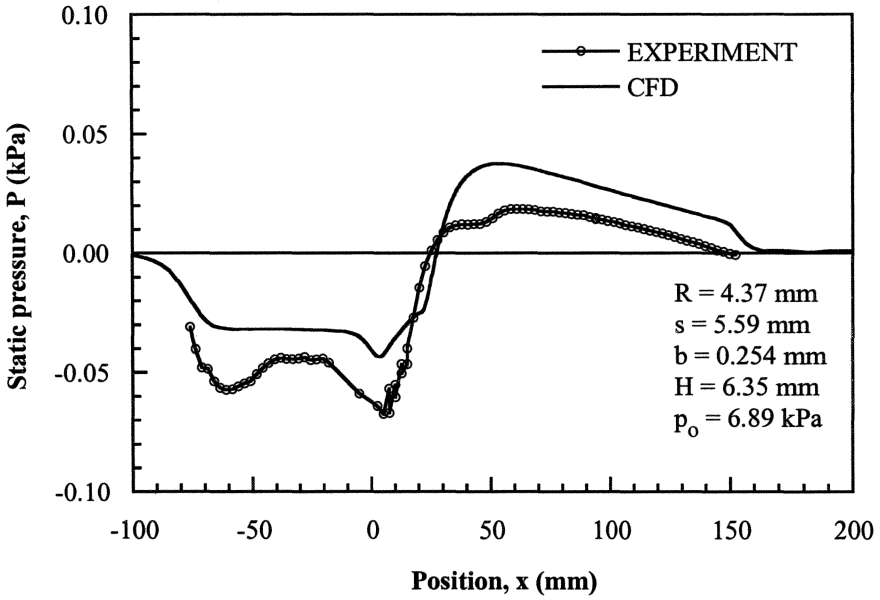


**Figure 21. Comparison of pressure profile on the rigid web**

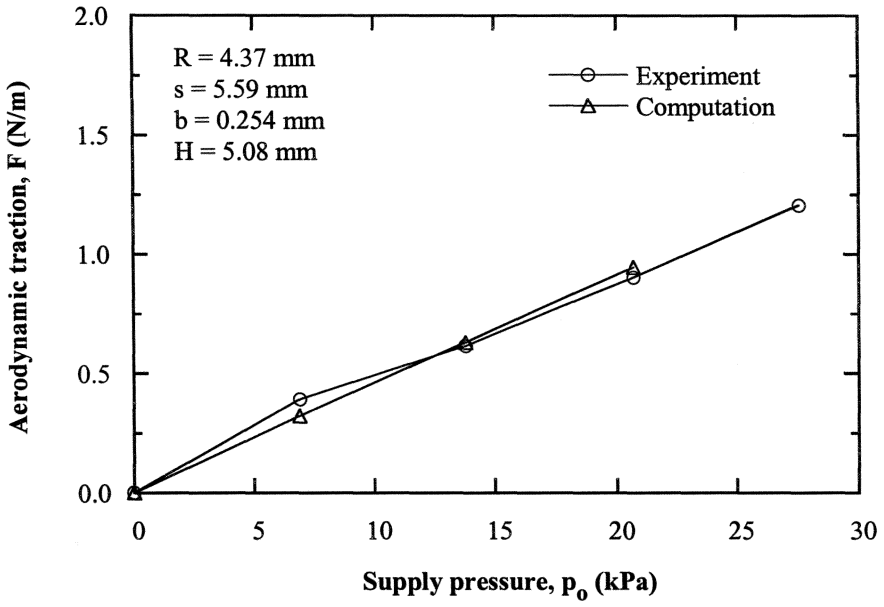


**Figure 22. Comparison of traction on the rigid web**

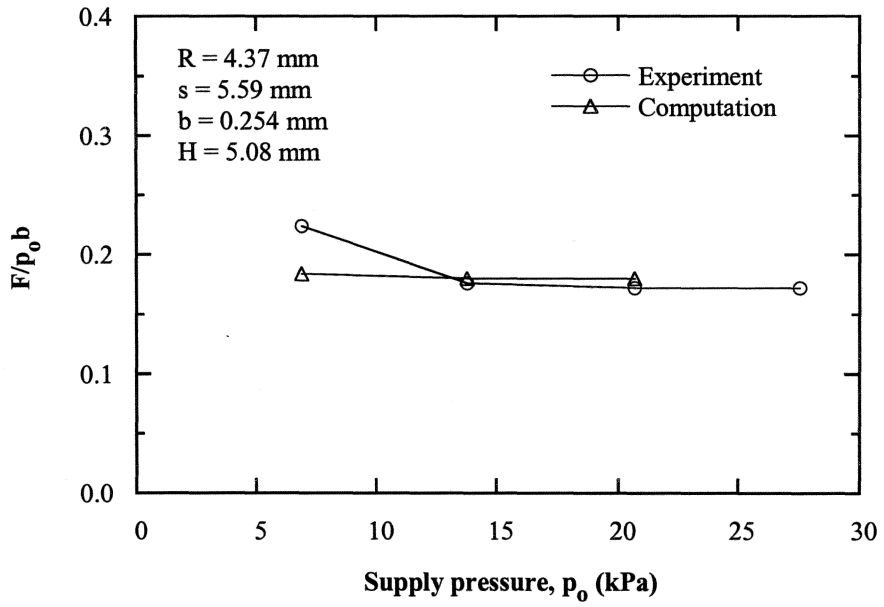


**Figure 23. Comparison of non-dimensional traction on the rigid web**

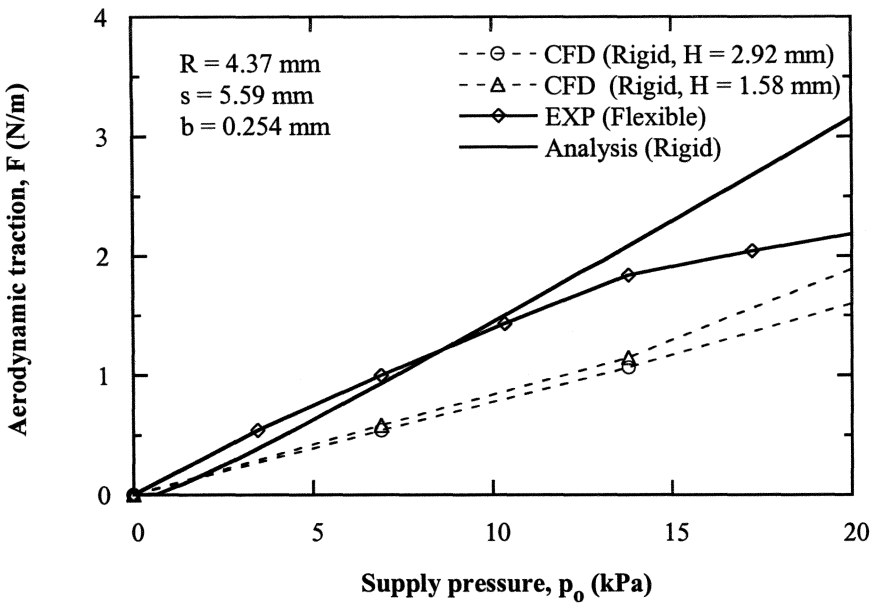


**Figure 24. Comparison of traction on the flexible web**

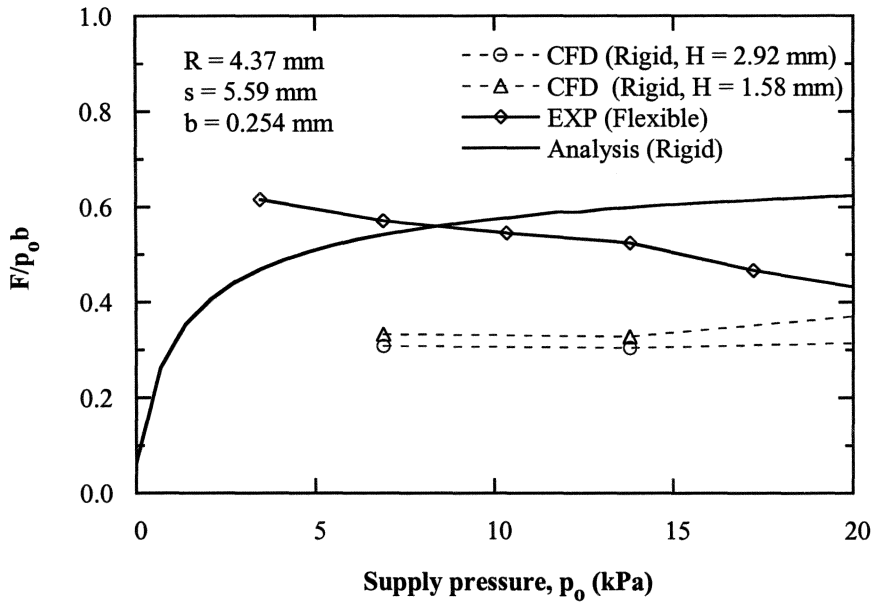


**Figure 25. Comparison of non-dimensional traction on the flexible web**

## SUMMARY AND CONCLUSIONS

An attempt was made to develop an analytical model to predict the aerodynamic traction on a rigid web subjected to the Coanda air jet. To fill the missing building blocks needed for the analysis, studies done for wall jets without the presence of the web were used, and also experimental results of the air jet traction were considered. Computations were done to determine the equilibrium position of a web and the air jet traction for the stationary rigid web, translating rigid web, stationary flexible web, and translating flexible web. The computational results were compared with the measurement data for a stationary flexible web. The following conclusions could be drawn from this study:

- There is an equilibrium position (flotation height) of a rigid web where the overall lift force becomes zero, and that equilibrium position is almost independent of the supply air pressure.
- The air jet traction on the web is almost proportional to the supply pressure.
- The air jet traction increases with the nozzle opening, the effect of nozzle opening is significant.
- The speed of web has significant effects on the interaction between the web and the air jet.
- When the air jet is in the machine direction (direction of web translation), the increase in web speed causes a reduction in the air jet traction.
- The effect of web speed on the air jet traction becomes less significant when the supply air pressure is high.
- The air jet traction on a flexible web is not strongly affected by web tension.
- If only a rough estimation of the air jet traction is needed for a stationary web, one may consider this relationship: $F / p_o b = 0.3 - 0.6$.

## ACKNOWLEDGMENT

This research has been supported by Web Handling Research Center at Oklahoma State University and its consortium members. The authors are grateful for their financial supports.

## REFERENCES

Aravamudhan, V. R., Moretti, P. M., and Chang, Y. B., "An Experimental Study of the Coanda Effect for 90° Turning of Subsonic Air Jets," Presented at the 1998 ASME Fluids Engineering Division Summer Meeting, June, 1998, Washington, DC.

Fujisawa, N. and Kobayashi, R. "Turbulence Characteristics of Wall Jets Along Strong Convex Surfaces," International Journal of Mechanical Sciences, Vol. 29, No. 5, 1987, pp. 311 – 320.

Hong, E. Y., "Aerodynamic Forces on a Web Subjected to the Coanda Air Jet," M. S. Thesis, Oklahoma State University, 1999.

Newman, B. G., "The Deflexion of Plane Jets By Adjacent Boundaries – Coanda Effect," Boundary Layer and Flow Control, Pergamon Press, Vol 1, 1961, pp. 232 - 264.

Reba, I., "Applications of the Coanda effect," Scientific American, Vol. 214, No. 6, 1966, pp. 84 - 92.

Rodman, L. C., Wood, N. J., and Roberts, L., "Experimental Investigation of Straight and Curved Annular Wall Jets," AIAA Journal, Vol. 27, No. 8, 1989, pp. 1059 - 1067.

Squire, H. A., "Jet Flow and Its Effects on Aircraft," Aircraft Engineering, Vol. 22, March 1950, pp. 62.

White, F. M., Viscous Fluid Flow, 2nd Edition, McGraw-Hill International Editions, 1974.

Wille, R. and Fernholz, H., "Report on the First European Mechanics Colloquium on the Coanda Effect," Journal of Fluid Mechanics, Vol. 23, No. 4, 1965, pp. 801 - 819.

Wilson, D. J. and Goldstein, R. J., "Turbulent Wall Jets With Cylindrical Streamwise Surface Curvature," Journal of Fluid Engineering – Transactions of the ASME, Vol. 98, No. 3, 1976, pp. 550 - 557.